https://doi.org/10.5194/egusphere-2026-13
Preprint. Discussion started: 14 January 2026

Promotion of Dense Shelf Water formation in the Ross Sea under the future trend of the Amundsen Sea Low

Zhaoru Zhang[*1,2,3,4], Heng Hu[1], Xiaoqiao Wang[5,6], Yuanjie Chen[1], Chuning Wang[1], and Chuan Xie[1]

[1] Key Laboratory of Polar Ecosystem and Climate Change, Ministry of Education; State Key Laboratory of Submarine Geoscience; School of Oceanography, Shanghai Jiao Tong University, Shanghai, China

[2] Shanghai Key Laboratory of Polar Life and Environment Sciences, Shanghai Jiao Tong University, Shanghai, China

[3] Shanghai Frontiers Science Center of Polar Science, Shanghai Jiao Tong University, Shanghai, China

[4] Key Laboratory for Polar Science, Polar Research Institute of China, Ministry of Natural Resources, Shanghai, China

[5] College of Meteorology and Oceanography, National University of Defense Technology, Changsha, China

[6] Key Laboratory of High Impact Weather (special), China Meteorological Administration, Changsha, China

[*] Corresponding author : Zhaoru Zhang

Email: zrzhang@sjtu.edu.cn

https://doi.org/10.5194/egusphere-2026-13
Preprint. Discussion started: 14 January 2026

ABSTRACT

The Amundsen Sea Low (ASL) is a k ow-pressure system influencing climate variability over West Antarctica. The Ross Sea is one of the major formation sites of Dense Shelf Water (DSW ecursor of the global ocean bottom water mass — Antarctic Bottom Water. This study uses CMIP6 multi-model ensemble means to project future changes in the ASL and the associated wind variations over the Ross and Amundsen Seas by the mid- and late-21st century. high-resolution coupled ocean-sea ice-ice shelf model covering the Ross Sea and the Amundsen Sea ~~is employed~~ to assess how these ASL-driven future wind changes affect DSW formation in the Ross Sea. By applying ASL-induced wind perturbations to three key regions that modulate the Ross Sea DSW characteristics, the respective contributions of regional wind-driven ocean-ice coupling processes to the DSW formation are quantified. The results show that the future deepening and southward shift of the ASL will enhance sea ice production in the Ross Sea polynyas and reduce meltwater inflow from Amundsen Sea ice shelves, thereby promoting DSW formation. Relative to present conditions, ASL-related wind changes over the Ross Sea and adjacent Amundsen Sea are projected to increase DSW production by approximately 8% by 2050 and 18% by 2100. These findings suggest that future ASL changes could help counteract the diminishing trend of DSW in the Ross Sea and maintain the Southern Ocean meridional overturning circulation.

Key words: Amundsen Sea Low, Dense Shelf Water, future variations, Ross Sea, Antarctica

Article Highlights:

- The future changes of ASL will enhance sea ice production in the Ross Sea polynyas.

https://doi.org/10.5194/egusphere-2026-13
Preprint. Discussion started: 14 January 2026

- The ASL variations will reduce ice shelf meltwater transport from the Amundsen Sea to the Ross Sea.

- Combined changes in sea ice production and meltwater transport will increase the Ross Sea DSW production in the future.

https://doi.org/10.5194/egusphere-2026-13
Preprint. Discussion started: 14 January 2026

1 Introduction

The Antarctic bottom water (AABW) plays a significant role in the global climate system by supplying the lower limb of the global meridional overturning circulation (Marshall and Speer 2012) and transporting carbon from polar regions to the deep oceans (De Lavergne et al., 2017; Sigman and Boyle, 2000). In the Pacific and Indian sectors of the Southern Ocean, AABW is supplied by the Ross Sea Bottom Water (RSBW) (Rintoul, 2007; van Wijk and Rintoul, 2014), which originates from the dense shelf water (DSW) primarily produced on the western Ross Sea continental shelf. The high salinity is the result of dramatic sea ice production in the coastal polynyas, including the Ross Ice Shelf polynya and the Terra Nova Bay polynya (Nihashi and Ohshima, 2015; Tamura et al., 2016; Jendersie et al., 2018; Zhang et al., 2025). Brine released during sea ice formation increases salinity of the surface waters, resulting in ocean deep convection and ultimately the formation of DSW in the polynya regions (Fusco et al., 2009).

In the past few decades, long-term hydrographic measurements in the Ross Sea have revealed a marked decrease in the salinity of DSW (Jacobs et al., 2002; Jacobs and Giulivi, 2010; Jacobs et al., 2022). Meanwhile, ice shelves in the Amundsen Sea are experiencing prominent increases in the basal melting over recent decades (Shepherd et al., 2018; Rignot et al., 2019). Most of the freshening in the Ross Sea has resulted from an increasing volume of ice shelf meltwater from the Amundsen Sea, which is transported westward to the Ross Sea by the Antarctic coastal and slope currents (Jacobs et al., 2022). Recent studies found that the DSW salinity rebounded after 2014 (Castagno et al., 2019), attributed to increased sea ice formation in the Ross Sea resulting from reduced ice transport from the Amundsen Sea (Silvano et al., 2020) or a reduction in freshwater transport from the Amundsen Sea (Guo et al., 2021). From the short-term and long-term changes in DSW salinity, it can be found that

https://doi.org/10.5194/egusphere-2026-13
Preprint. Discussion started: 14 January 2026

sea ice production in coastal polynyas in the Ross Sea and the freshwater input from the Amundsen Sea are the two most important processes affecting the DSW formation in the Ross Sea.

Winds over the Ross Sea and Amundsen Sea ~~could~~ affect both sea ice formation in the Ross Sea polynyas and the transport of meltwater from the Amundsen Sea, and further affect ~~the~~ DSW formation in the Ross Sea. Polynyas in the Ross Sea are formed and maintained by strong offshore katabatic winds that are generated by the steep terrain along the coast (Bromwich and Kurtz, 1984; Park et al., 2018). The offshore winds drive sea ice away from the coast, increasing the open water area of the polynyas and leading to more ice production due to intense oceanic heat loss to the atmosphere. Offshore winds can also be generated by large-, synoptic- and meso-scale atmospheric circulations (Chenoli et al., 2015; Weber et al., 2016; X. Wang et al., 2021; X. Wang et al., 2023; Zhang et al., 2024). The western Amundsen Sea is a key region for the transport of meltwater and sea ice from the Amundsen Sea into the Ross Sea (Nakayama et al., 2014; Xie et al., 2024; Xie et al., 2025). Easterly winds over the western Amundsen Sea drive onshore Ekman transport and create a doming of the sea surface and deepening of the pycnocline near the coast, thereby intensifying the westward coastal flows (Kim et al., 2016; Dotto et al., 2018) that are crucial for the freshwater and ice transports. In the eastern Amundsen Sea, zonal winds over the slope can modulate the on-shelf intrusion of warm Circumpolar Deep Water (CDW), with stronger westerly winds leading to greater CDW intrusion (Thoma et al., 2008; Wåhlin et al., 2013; Jenkins et al., 2018; Li et al., 2025). The intruded CDW can be transported all the way to the ocean cavities beneath ice shelves and cause basal melting (Paolo et al., 2015; Konrad et al., 2018). Nakayama et al. (2014) revealed that a slight increase of the basal mass loss in the Amundsen Sea rapidly intensifies the basal meltwater transport downstream into the Ross Sea.

https://doi.org/10.5194/egusphere-2026-13
Preprint. Discussion started: 14 January 2026

The Amundsen Sea Low (ASL) is a climatological low-pressure system in the high-latitude South Pacific sector of the Southern Ocean (Fig. 1), which covers the Ross Sea, the Amundsen Sea, and the Bellingshausen Sea (Turner et al., 2013; Coggins and McDonald, 2015; Raphael et al., 2016). It is strongly influenced by large-scale patterns of atmospheric variability, such as the Southern Annular Mode (SAM) and El Niño Southern Oscillation (ENSO) (Clem et al., 2017; Li et al., 2021). It has profound impacts on the atmospheric circulations over the Ross Sea and Amundsen Sea regions, which will further impact the sea ice fields and oceanic circulations (Holland et al., 2018; Raphael et al., 2019; Dotto et al., 2020; T. Wang et al., 2021; S. Wang et al., 2023). By modulating the wind field over the Ross Sea region, a deeper and more eastward ASL in November may result in a larger and more eastward-located Ross Ice Shelf polynya in December (T. Wang et al., 2022). Guo et al. (2021) demonstrated that the accelerated deepening of the ASL and the resulting southwestward extension of low pressure induces eastward coastal current anomalies and reduces the freshwater input from the Amundsen Sea to the Ross Sea, which is responsible for the subsequent increase of DSW salinity in the western Ross Sea in recent years. Dotto et al. (2020) suggested that the fate of the West Antarctic ice shelves is closely tied to the evolution of the ASL by establishing a link between heat content on the Amundsen Sea shelf and local wind associated with the ASL. In the future, the ASL is projected to deepen and migrate poleward significantly under high-level warming scenarios based on the Coupled Model Intercomparison Project Phase 5 and 6 (CMIP5/6) models (Hosking et al., 2016; Gao et al., 2021), which will influence the atmospheric circulations over the Ross Sea and the Amundsen Sea and can induce changes in sea ice production, ice shelf basal melting and the transport of meltwater from the Amundsen Sea, all of which will possibly affect the formation of DSW in the Ross Sea. Up until now, the impacts of the future ASL changes on the DSW formation have not been revealed, which is the objective of this study.

https://doi.org/10.5194/egusphere-2026-13
Preprint. Discussion started: 14 January 2026

In this work, a high-resolution coupled ocean-sea ice-ice shelf model covering the Ross Sea and Amundsen Sea was developed to investigate the effects of future wind changes related to the ASL change on the DSW formation in the Ross Sea. Multi-model ensemble mean results from CMIP6 were used to project the future changes of ASL properties, and the projected changes in wind caused by the ASL variation were obtained based on the statistical relationship between the two quantities over the historical period. Sensitivity experiments were conducted by applying wind perturbations associated with ASL changes over the Ross Sea shelf, the western Amundsen Sea, and the eastern Amundsen Sea shelf and slope region respectively. Changes in DSW production in the Ross Sea in these experiments were quantified and the physical mechanisms for these changes were revealed.

2 Methodology

2.1 Numerical model

The high-resolution ocean-sea ice-ice shelf model of the Ross Sea and Amundsen Sea employed in this study, named the **R**oss-**A**mundsen Sea **I**ce-**Se**a Model (RAISE; Zhang et al., 2025), was developed based on the Regional Ocean Modeling System (ROMS). ROMS is a free-surface, terrain-following coordinate, primitive equations ocean circulation model developed for coastal ocean modeling studies (Haidvogel et al., 2008; Shchepetkin and McWilliams, 2009). The model domain (Fig. 1) extends from roughly 85.6°S to 64.2°S and from 143.0°E to 89.9°W, which covers the entire Ross Sea and the Amundsen Sea, including the portion underneath the floating ice shelves. The model horizontal resolution varies from ~2 km in the coastal regions to ~6 km in the open ocean. The model includes 32 vertical levels that are concentrated near the surface and the sea floor.

https://doi.org/10.5194/egusphere-2026-13
Preprint. Discussion started: 14 January 2026

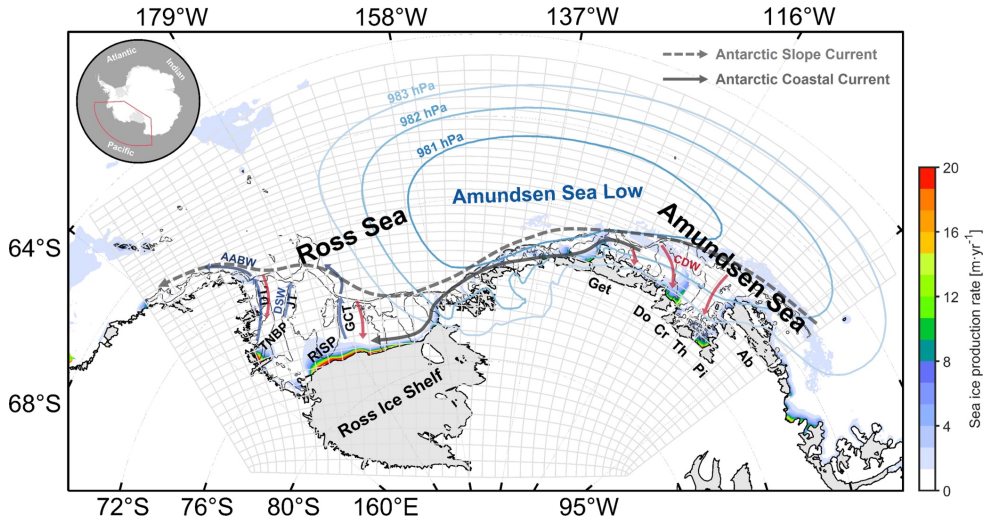

Figure 1. Domain and grid of the coupled ocean-sea ice-ice shelf model (RAISE) over the Ross Sea and the Amundsen Sea. The inset shows the location of model domain in the Southern Ocean. The isobars indicate the climatological condition of the Amundsen Sea Low (ASL). The blue arrows indicate the movement of Dense Shelf Water (DSW) and Antarctic Bottom Water (AABW), while the red arrows indicate the movement of Circumpolar Deep Water (CDW). The color indicates the sea ice production rate. The Terra Nova Bay polynya (TNBP) and Ross Ice Shelf polynya (RISP) are labeled. The gray areas indicate ice shelves. Local ice shelves including the Abbot Ice Shelf (Ab), Pine Island Ice Shelf (Pi), Thwaites Ice Shelf (Th), Crosson Ice Shelf (Cr), Dotson Ice Shelf (Do), and Getz Ice Shelf (Get) are labeled. The gray lines indicate the 500-m and 1000-m isobaths.

The model bathymetry and ice shelf draft have been interpolated from BedMachine-Antarctica-v2.0 (Morlighem et al., 2020), which has a spatial resolution of 500 m on the Antarctic Polar Stereographic projection. Sea ice is simulated with a dynamic sea ice model (Budgell 2005) coupled with the ROMS model. The ice dynamics are based on elastic–viscous–plastic rheology (Hunke and Dukowicz 1997; Hunke 2001). The ice thermodynamics

https://doi.org/10.5194/egusphere-2026-13
Preprint. Discussion started: 14 January 2026

are described by Mellor and Kantha (1989) and Häkkinen and Mellor (1992). In this model, sea ice is represented by two layers and temperature gradients within the ice are allowed. A snow layer is included, which acts as an insulating layer and changes the surface albedo. This model also includes the mechanical and thermodynamic effects of ice shelves on the waters beneath based on the three-equation parameterization (Holland and Jenkins, 1999; Dinniman et al., 2011). The ice shelves in the model are static, and there is no mass variation of the ice shelf or any iceberg calving parameterization. Vertical mixing of momentum and tracers are computed using the K-profile parameterization (KPP) mixing scheme (Large et al., 1994).

Atmospheric forcings for this model come from the ERA5 reanalysis product (Hersbach et al., 2020), which include wind speed, sea level pressure, humidity, air temperature, cloud cover and precipitation. The atmospheric forcing fields use 3-hourly data for wind and air temperature, and daily data for other variables. Initial conditions of temperature and salinity are taken from the 10-km horizontal-resolution circum-Antarctic ocean-sea ice-ice shelf model (Dinniman et al., 2015). The temperature, salinity, sea surface height, and depth-averaged velocity for the open boundaries are derived from daily mean data produced by the Met Office Global Seasonal forecasting system version 5 (GloSea5) (Maclachlan et al., 2015). Daily sea ice concentration boundary conditions are obtained from the Advanced Microwave Scanning Radiometer-Earth Observing System (AMSR-E) and Advanced Microwave Scanning Radiometer 2 (AMSR2) dataset provided by the University of Bremen using the ARTIST sea ice algorithm (Spreen et al., 2008). Tidal forcing is derived from the global tidal solution TPXO9 (Egbert and Erofeeva 2002), including 15 major tidal constituents (K1, S2, M4, P1, O1, Q1, S1, MS4, MN4, MF, 2N2, M2, K2, MM and N2), forced at the open boundaries through sea surface height and barotropic currents.

https://doi.org/10.5194/egusphere-2026-13
Preprint. Discussion started: 14 January 2026

In this study, a base simulation (named Present simulation) is obtained by initializing the model from a 7-yr spin-up simulation from 1998 to 2004 and integrating it from 2005 to 2014. Extensive validation of the base simulation has been presented in Zhang et al. (2025), Zhang et al. (2024) and Xie et al. (2024), confirming the model's strong capability in reproducing key physical processes associated with DSW production and transport in the Ross Sea and Amundsen Sea. ~~The~~ simulations successfully capture the sea-ice and DSW production rates within the Ross Sea polynyas, the DSW export rates at the trough exits, the temporal evolution of DSW salinity and density as well as the ice shelf melting rates in the Amundsen Sea. The simulated interannual variability of DSW salinity near the Ross Ice Shelf polynya is significantly correlated with that from 17-year on-site observational data ($R=0.66$, p-value=0.004), and the simulated variability of DSW neutral density at a major DSW export outlet in the Ross Sea is highly correlated with that from 4-year mooring measurements ($R=0.75$, p-value<0.001) (Zhang et al., 2025).

2.2 Sensitivity experiments

2.2.1 Deriving the relation between long-term variability of the ASL and wind

Following Hosking et al. (2013), three indices are used to describe the ASL depth and positions, including the actual central pressure (ACP), longitude (LON) and latitude (LAT). The ASL center is defined as the location with minimum MSLP value over the ASL sector (170–298°E, 80–60°S) following Hosking et al. (2016). In this study, annual ASL indices are defined by the annual mean sea level pressure (MSLP) from ERA5 for the present period or CMIP6 for the future periods.

To describe the relationship between variations of ASL indices and wind speed over the study areas on interdecadal timescales (~10 years), we performed a correlation analysis between the anomalies of ASL indices and each wind component for the period 1959–2021

https://doi.org/10.5194/egusphere-2026-13
Preprint. Discussion started: 14 January 2026

using the ERA5 product (Fig. 2). The anomaly time series are smoothed with a 10-year running mean to extract the interdecadal variability following Henley et al. (2015), and effective degrees of freedom are used to test the significance of correlation (Bretherton et al., 1999). For the sensitivity experiments described in the next section, wind changes associated with the future variations of ASL indices are added to the atmospheric forcings over three crucial regions, which exhibit significant correlations between the ASL indices and wind as illustrated in Fig. 2. The first region is the central Ross Sea shelf, which includes one important formation site for the DSW formation — the Ross Ice Shelf polynya (166–194°E and 76.5–78.5°S). A significant negative correlation exists between the variations of meridional wind component and ASL-ACP (Fig. 2b). Therefore, in the sensitivity experiment we would consider the perturbations of meridional wind component caused by the ASL-ACP variation in this area. The second region is the western Amundsen Sea (referred to as WAS and denoted as region B in Fig. 2e, spanning 200–228°E and 73.25–77.25°S), which is the key region for westward transport of ice shelf meltwater from the Amundsen Sea to the Ross Sea (Silvano et al., 2020). The third region is the eastern Amundsen Sea shelf and slope region (referred to as EASS and denoted as region C in Fig. 2e, spanning 230–262°E and 70.5–73.5°S), where zonal winds can significantly affect the on-shelf intrusion of CDW and thus melting of major ice shelves in the Amundsen Sea (Jenkins et al., 2018; Silvano et al., 2022). In both the second and third regions, significant negative correlations exist between the ASL-LAT and the zonal wind speed (Fig. 2e), while the correlations between ASL indices and the meridional wind are not significant (Figs. 2b,d,f,h). As such, in the sensitivity experiments we apply perturbations of zonal winds associated with the ASL-LAT variability to the atmospheric forcings over these two regions. ASL is also shown to modulate air temperature and moisture advection via control of winds over the West Antarctica (Nicolas and Bromwich, 2011; Bromwich et al., 2011) and the Ross

https://doi.org/10.5194/egusphere-2026-13
Preprint. Discussion started: 14 January 2026

228 Sea (Cohen et al., 2013). However, our analysis reveals no significant correlations between
229 variations in air temperature or humidity and ASL properties across the three regions.

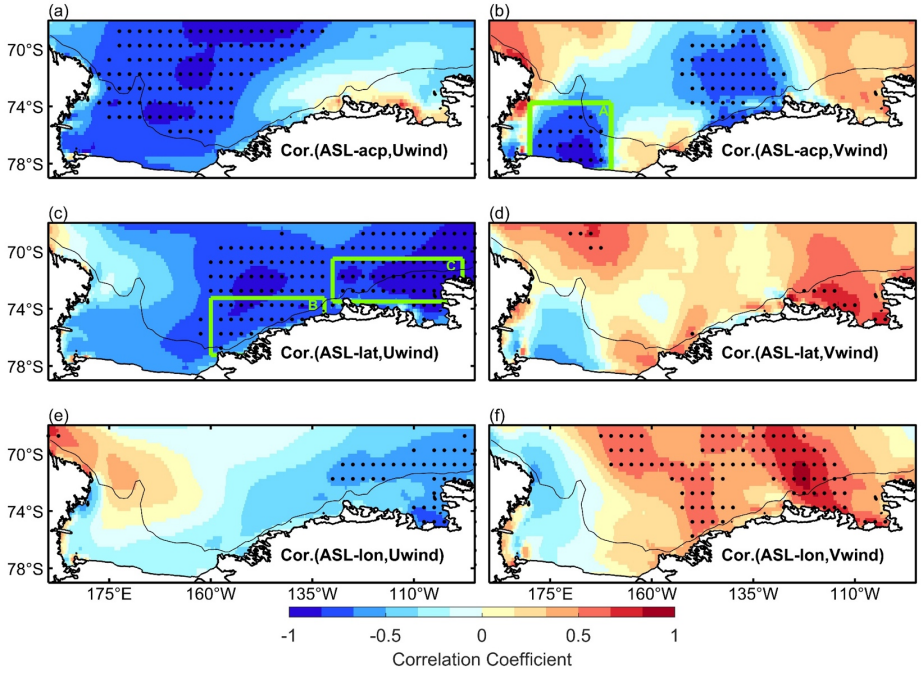

230

231 **Figure 2.** (a, c, e) Spatial distributions of correlation coefficients between the interdecadal
232 variability of zonal wind anomalies and (a) ASL-ACP, (c) ASL-LAT and (e) ASL-LON
233 anomalies. (b, d, f) Spatial distributions of correlation coefficients between the interdecadal
234 variability of meridional wind anomalies and (b) ASL-ACP, (d) ASL-LAT and (f) ASL-LON
235 anomalies in the Ross Sea and Amundsen Sea. All anomaly time series are smoothed with a
236 10-year running mean from 1959 to 2021. The green boxes show the three key regions where
237 wind perturbations associated with the ASL changes are applied in the sensitivity experiments.
238 Dots represent correlations significant at the 95% confidence level. The thin black line
239 indicates the 1000-m isobath.

240 **2.2.2 The projection of future ASL changes based on CMIP6 models**

https://doi.org/10.5194/egusphere-2026-13
Preprint. Discussion started: 14 January 2026

Gao et al. (2021) evaluated historical simulations of climatological characteristics of ASL in CMIP5 and CMIP6 against the ERA5 reanalysis product. Both the spatial distribution and annual cycle of ASL are improved in CMIP6 multi-model ensemble mean compared to CMIP5, and the dispersion of ASL-ACP, ASL-LAT, and ASL-LON simulated by CMIP6 models are much smaller than those in CMIP5. Here, we used the ERA5 product to validate the representation of ASL-ACP (Fig. 3a), LAT and LON (Fig. 3b) in the historical simulations (1850–2014) of 34 CMIP6 models during 1959–2014. 10 models with the lowest root mean square deviations (RMSD) in the ASL-ACP, LAT and LON were selected, which are EC-Earth3, BCC-CSM2-MR, NorESM2-LM, CMCC-ESM2, GFDL-ESM4, CIESM, FIO-ESM-2-0, HadGEM3-GC31-MM, E3SM-1-0 and TaiESM1 (Figs. 3a,b).

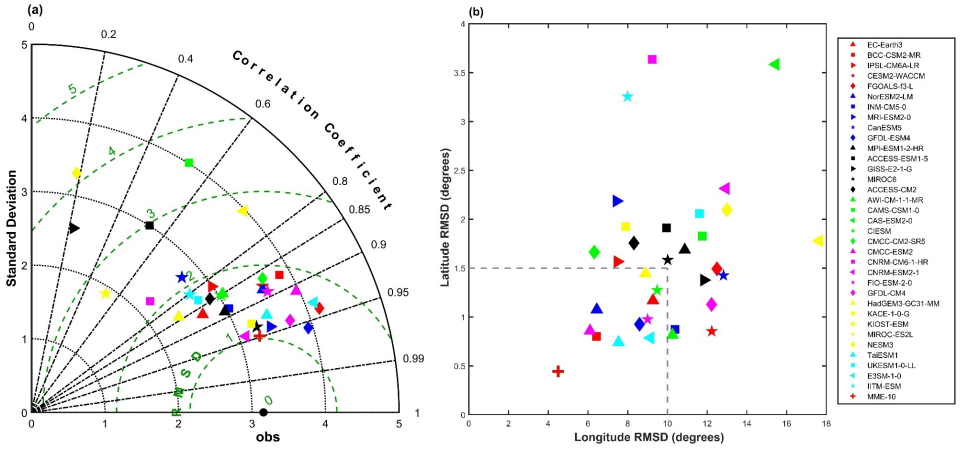

Figure 3. (a) Taylor diagram of the actual central pressure of the ASL (ACP) in CMIP6 models against the ERA5 product during 1959–2014. (b) Scatterplot of the root mean square deviations (RMSD) for 34 CMIP6 models relative to ERA5 for longitude (LON) and latitude (LAT) of the ASL over the period 1959–2014. 10 models with the lowest RMSD values in both the ASL LAT and LON (those that lie within the dashed lines) are selected. Red cross denotes the value of the 10-model-mean (CMIP6-MME10) in this study.

https://doi.org/10.5194/egusphere-2026-13
Preprint. Discussion started: 14 January 2026

Using the ensemble mean results of the 10 models (named as CMIP6-MME10) selected above, we examined how the ASL indices will change under a high-emission scenario — SSP585 in the future. The projected ASL features were examined for two 10-year periods respectively in the middle (2051–2060) and end (2091–2100) of the twenty-first century. The CMIP6-MME10 MSLP for the present period (2005–2014), 2051–2060 and 2091–2100 are shown in Figs. 4a, 4b, and 4c, respectively. The differences in the ASL indices in the future periods compared to the present period are listed in Table 1. The changes in ACP are significant, which are 1.27 hPa and 2.87 hPa deeper in 2051–2060 and 2091–2100 than the present period, respectively. The ASL will move southward by 0.38° in 2051–2060 and 1.01° in 2091–2100, respectively, while no significant changes in the ASL longitude are found.

Table 1. Projected changes of ASL central pressure (ACP), latitude (LAT) and longitude (LON) from CMIP6-MME10 under the SSP585 scenario relative to the present period (2005–2014). Stars denote changes significant at the 95% confidence level.

	2005–2014	**2051–2060**	**2091–2100**
ACP (hPa)	976.95	975.68*	974.08*
LAT (°S)	71.60	71.98	72.61*
LON (°E)	221.04	221.20	218.86

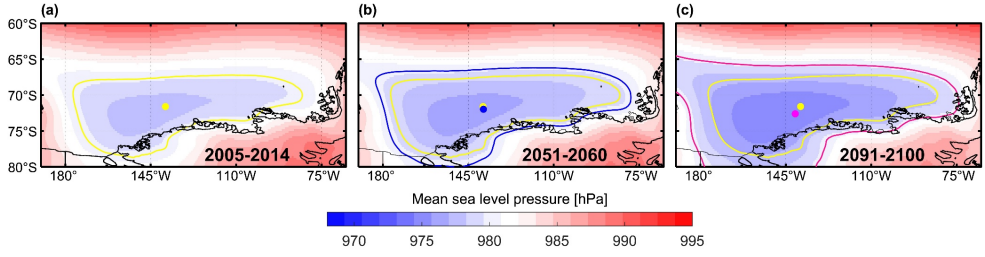

https://doi.org/10.5194/egusphere-2026-13
Preprint. Discussion started: 14 January 2026

Figure 4. Mean sea level pressure from CMIP6-MME10 during (a) 2005–2014, (b) 2051–2060 and (c) 2091–2100. The yellow, blue and magenta contour lines and dots denote the 980-hPa isobar and the central location of the ASL during 2005–2014, 2051–2060 and 2091–2100, respectively.

2.2.3 Wind perturbation sensitivity experiments

Linear relations between the anomalies of wind speed and ASL indices are derived for each of the three regions using the ERA5 reanalysis from 1959 to 2021, as shown in Fig. 5. Then, based on these relations and projected changes in the depth and position of ASL from CMIP6-MME10, changes in wind associated with the ASL index variation for each of the three regions relative to the present period are derived. Over the Ross Sea shelf, a deeper ASL results in an increase in southerly wind by 2.9% for 2051–2060 and 7.3% for 2091–2100 (Fig. 5a). Over the WAS, the average easterly wind is projected to decrease by 2.1% for 2051–2060 and 9.4% for 2091–2100 compared to present period under the southward shift of the ASL (Fig. 5b). Over the EASS, the average easterly wind will decrease by 17.3% for 2051–2060 and 33.2% for 2091–2100 as the ASL shifts southward (Fig. 5c).

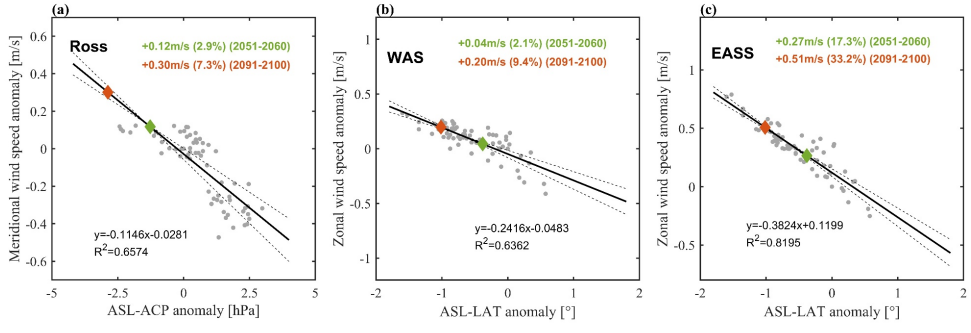

https://doi.org/10.5194/egusphere-2026-13
Preprint. Discussion started: 14 January 2026

Figure 5. Linear regression between the anomalies of annual wind speed and ASL indices in 1959–2021 over (a) the Ross Sea shelf (Ross), (b) the western Amundsen Sea (WAS) and (c) the eastern Amundsen slope and shelf (EASS). The coefficient of determination (R^2) and regression equation are shown in each panel. The gray dotted line in each panel denotes the uncertainty range of the regression slope at the 95% confidence interval. The green and orange diamonds on the dashed lines represent the projections of ASL indices based on CMIP6-MME10 for 2051–2060 and 2091–2100, respectively. The green and orange numbers in each panel are the projected changes of wind speed derived from the linear relationship for the periods 2051–2060 and 2091–2100, respectively. The percent changes in the wind speed relative to the values in the present period are shown in brackets in each panel.

~~Numerical~~ ~~s~~ensitivity experiments were conducted by applying the projected wind changes associated with the ASL variations to the atmospheric forcing fields for the Present simulation over each of the three key regions. In addition, we also applied wind perturbations over these three regions simultaneously to study the overall changes in the DSW formation (the experiments are named "Total"). Configurations of these experiments are summarized in Table 2. Modifications were made to the present wind field via scaling each wind component by a constant factor estimated from Fig. 5. Except for wind, other atmospheric forcing variables and boundary conditions are the same as in the Present simulation. In the model we also set dyes for meltwater originating from basal melting of ice shelves in the Amundsen Sea, to trace the meltwater transport into the Ross Sea. The content of the dye release is proportional to the melting rate of the ice shelf at each grid following Xie et al. (2024).

https://doi.org/10.5194/egusphere-2026-13
Preprint. Discussion started: 14 January 2026

314 **Table 2.** Summary of the configurations for the Present simulation and sensitivity experiments.

Experiment	Region for applying the wind field perturbation	Simulation period	Wind perturbation related to the ASL change
Present	/	2005–2014	/
Ross-2050F	Ross Sea shelf	2051–2060	Southerly×(1+2.9%)
Ross-2100F		2091–2100	Southerly×(1+7.3%)
WAS-2050F	Western Amundsen Sea	2051–2060	Easterly×(1-2.1%)
WAS-2100F		2091–2100	Easterly×(1-9.4%)
EASS-2050F	Eastern Amundsen Sea shelf and slope	2051–2060	Easterly×(1-17.3%)
EASS-2100F		2091–2100	Easterly×(1-33.2%)
Total-2050F	Ross Sea shelf, Western Amundsen Sea and Eastern Amundsen Sea shelf and slope	2051–2060	All of the wind perturbations above
Total-2100F		2091–2100	

315 All simulations start from the end of the 5-yr spin-up simulation for the base simulation
316 mentioned in Section 2 and are integrated for 5 years. Unless explicitly stated, all results
317 analyzed below are from the last year of each simulation, which represent the most stable ocean
318 state.

319 **3 Results**

https://doi.org/10.5194/egusphere-2026-13
Preprint. Discussion started: 14 January 2026

3.1 Changes in DSW formation caused by ASL-induced wind changes over the Ross Sea continental shelf

As shown in Fig. 6a, the majority of DSW (defined as neutral density $\gamma^n > 28.27$ kg m^{-3}) in the Ross Sea is formed within the Terra Nova Bay polynya and the western section of the Ross Ice Shelf polynya. For the Ross-2050F and Ross-2100F simulations, under the enhanced southerly winds, which are offshore winds for the Ross Ice Shelf polynya, sea ice production in the Ross Sea during the ice freezing season (March–October) increased by 19.8 km^3 yr^{-1} and 51.2 km^3 yr^{-1}, respectively. The changes in sea ice production directly affect the DSW formation through salt release. Differences between the DSW layer thicknesses in Ross-2050F/Ross-2100F and the Present simulation over the Ross Sea shelf are shown in Figs. 6b,c. Substantial increases in the DSW layer thicknesses are observed over the majority of the western Ross Sea in Ross-2050F/Ross-2100F, with the most pronounced increases present in the western Ross Ice Shelf polynya and the Terra Nova Bay polynya. The DSW volume over the Ross Sea shelf in the Ross-2050F and Ross-2100F simulations are greater than that at present by 1.6% and 8.8%, respectively (Table 3). We also selected three transects (S1, S2 and S3 in Fig. 6a) across three troughs — the Drygalski Trough (DT), the Joides Trough (JT) and the Glomar Challenger Trough (GCT) that are major passages for the DSW outflows, and calculated the total DSW exports toward the slope through these transects. The DSW exports in Ross-2050F show a slight increase (3.4%) compared to the Present simulation and a notable increase (8.5%) in Ross-2100F, rising from 1.18 Sv in the Present simulation to 1.22 Sv and 1.28 Sv, respectively. Increases in DSW exports in Ross-2100F are primarily concentrated in GCT and JT, contributing 70% and 20% of the total increase, respectively.

Table 3. Mean DSW volume on the Ross Sea shelf in different simulations. The numbers in brackets show the changes as proportions of the DSW volume relative to the present.

https://doi.org/10.5194/egusphere-2026-13
Preprint. Discussion started: 14 January 2026

Simulation	Present	Ross-2050F	Ross-2100F	WAS-2050F	WAS-2100F
DSW volume (10^4 km^3)	4.34	4.41 (+1.6%)	4.72 (+8.8%)	4.43 (+2.1%)	4.62 (+6.5%)

Simulation	EASS-2050F	EASS-2100F	Total-2050F	Total-2100F
DSW volume (10^4 km^3)	4.54 (+4.6%)	4.57 (+5.3%)	4.66 (+7.4%)	5.07 (+16.8%)

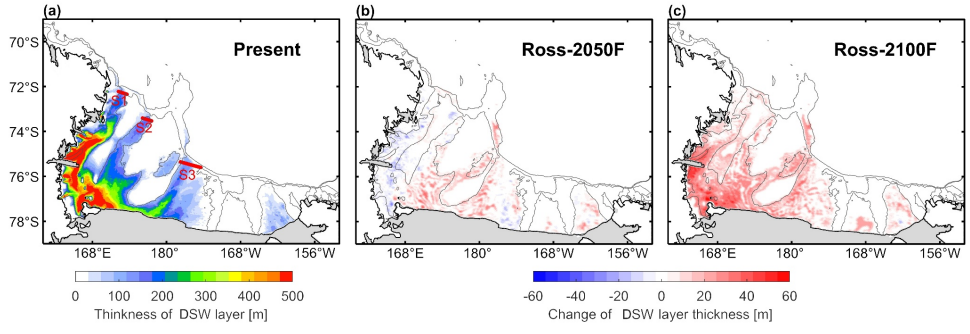

Figure 6. (a) Spatial distributions of the DSW layer thickness in the Ross Sea for the Present simulation. Changes in DSW layer thicknesses for (b) Ross-2050F and (c) Ross-2100F relative to the Present simulation. The red lines in (a) indicate the S1, S2 and S3 transects, and the gray lines indicate the 500-m and 1000-m isobaths.

3.2 Changes in ice shelf meltwater transport in the western Amundsen Sea and the impacts on DSW production

https://doi.org/10.5194/egusphere-2026-13
Preprint. Discussion started: 14 January 2026

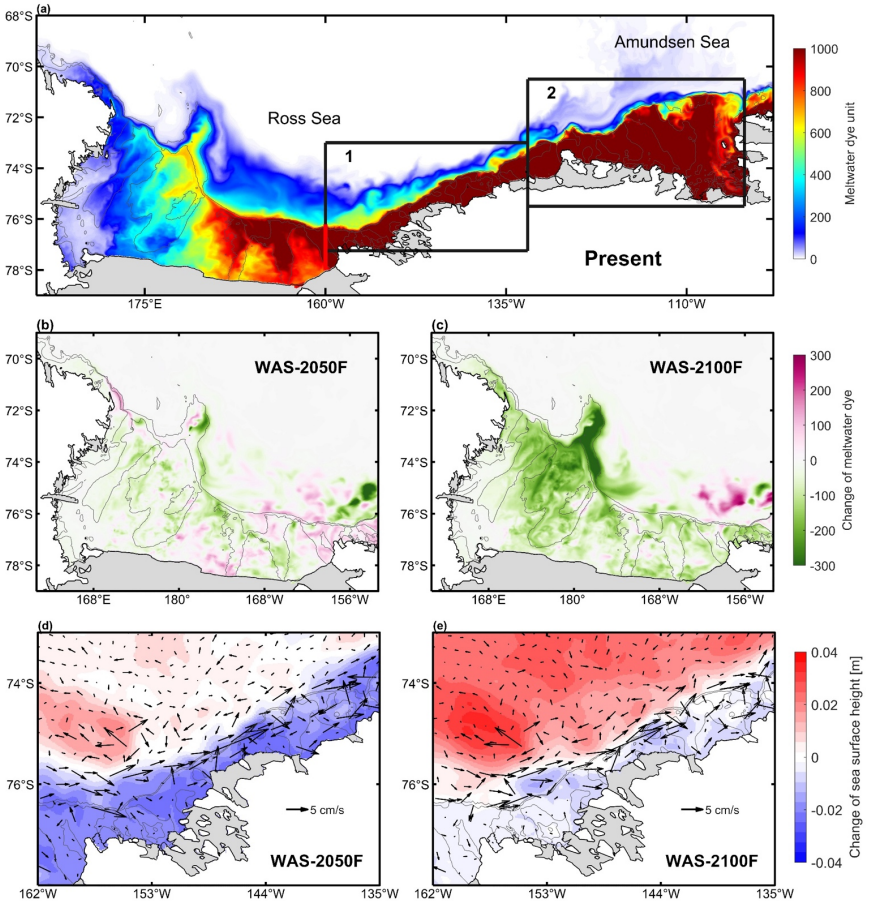

352

353 **Figure 7.** (a) Spatial distributions of meltwater dye unit released from the Amundsen Sea ice
354 shelves in the last year of the Present simulation. Changes in the meltwater dye unit over the
355 Ross Sea for the (b) WAS-2050F, (c) WAS-2100F simulations relative to the Present
356 simulation. Changes in sea surface height (SSH) from the (d) WAS-2050F and (e) WAS-2100F
357 simulations relative to the Present simulation, with changes in barotropic currents
358 superimposed. Black Box 1 in (a) indicates the region plotted for (d) and (e). Black Box 2 in
359 (a) indicates the region plotted for Figs. 8c and 8d. The red line in (a) represents the gate used
360 to estimate the sea ice import from the Amundsen Sea into the Ross Sea. Isobaths of 500-m
361 and 1000-m are shown by the black thin lines.

https://doi.org/10.5194/egusphere-2026-13
Preprint. Discussion started: 14 January 2026

The dyes for tracing meltwater from the Amundsen Sea ice shelves clearly show westward spreading in the Present simulation (Fig. 7a). For all simulations, meltwater is transported to the Ross Sea shelf within 3 years after the dyes are released. In the future, the southward shift of the ASL lead to a weakening of the easterly winds over the WAS (Fig. 5c and Table 2). This results in a decrease in the amount of meltwater dyes entering the Ross Sea (Figs. 7b,c) compared to the Present simulation, by 4.2% and 18.1% in WAS-2050F and WAS-2100F, respectively. The reason for the decreased transport is that the weakened easterly winds decreases the southward Ekman transport, reducing the cross-shelf sea surface height (SSH) gradient and the westward barotropic coastal currents (Figs. 7d,e). As fresh meltwater from the Amundsen Sea partially offsets the salt flux by sea ice formation in the Ross Sea polynyas and inhibits the DSW formation (Silvano et al., 2018; Xie et al., 2025), the reduced meltwater transport to the Ross Sea results in an increase of the mean DSW volume in the Ross Sea by 2.1% in WAS-2050F and 6.5% in WAS-2100F (Table 3). The DSW transports toward the slope across the three transects in troughs increase by 2.5% and 10.2% in WAS-2050F and WAS-2100F, respectively.

3.3 Changes in CDW intrusion and ice shelf melting in the eastern Amundsen Sea and impacts on the DSW production

In the future, the southward shift of ASL will lead to a weakening of easterly winds over the eastern Amundsen Sea shelf and slope (Fig. 5d). In EASS-2050F and EASS-2100F, the easterly wind anomalies over the slope of the Amundsen Sea will enhance the eastward barotropic currents (Figs. 8a,b), intensifying the eastward undercurrents in this area (Figs. 8c,d) that would enhance the CDW intrusion based on previous studies (Wåhlin et al., 2013; Dotto et al., 2020; Li et al., 2025). The potential temperature at 450 m in the CDW core layer on the

https://doi.org/10.5194/egusphere-2026-13
Preprint. Discussion started: 14 January 2026

385 Amundsen Sea shelf shows a significant increase, indicating stronger CDW intrusion (Figs.
386 8e,f).

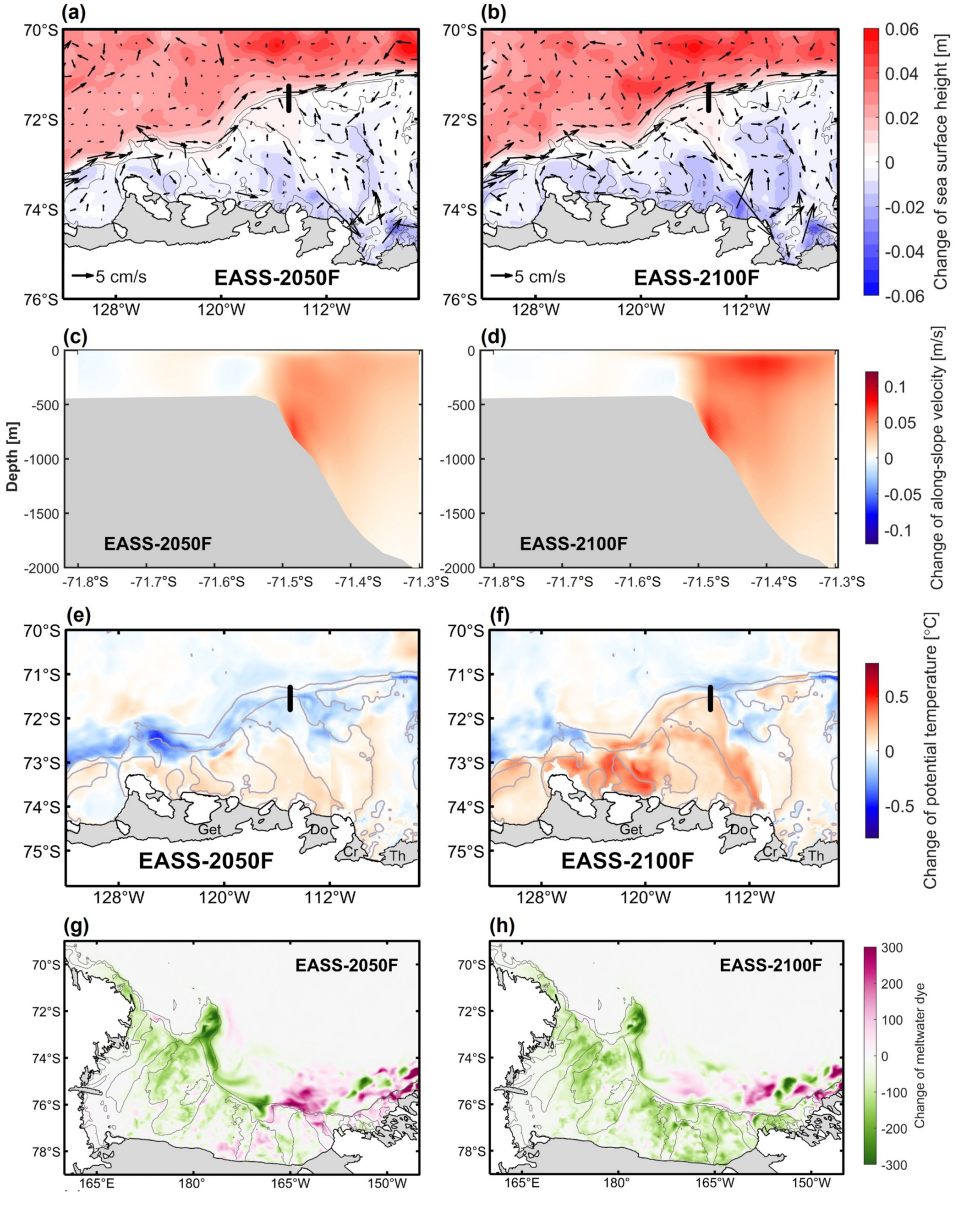

387

388 **Figure 8.** Changes in sea surface height (SSH) in the (a) EASS-2050F and (b) EASS-2100F
389 simulations relative to the Present simulation, with changes in barotropic currents

https://doi.org/10.5194/egusphere-2026-13
Preprint. Discussion started: 14 January 2026

superimposed. (c, d) Vertical sections (see the section locations indicated as black lines in a and b) of along-slope velocity changes (m s^{-1}) in the (c) EASS-2050F and (d) EASS-2100F simulations relative to the Present simulation. The positive value denotes eastward velocity. (e, f) Changes of potential temperature (°C) at 450 m in the Amundsen Sea in the (e) EASS-2050F and (f) EASS-2100F simulations. (g,h) Changes in meltwater dye units over the Ross Sea for the (g) EASS-2050F and (h) EASS-2100F simulations relative to the Present simulation. Isobaths of 500-m and 1000-m are shown by the gray thin lines.

Heat content of the CDW layer on the Amundsen Sea shelf (230–260°E, south of 73°S) is calculated from the temperature above the in-situ freezing point below 350 m over the Amundsen Sea (Jacobs et al., 2011; Nakayama et al., 2013), based on the equation used in Dotto et al. (2020). In EASS-2050F and EASS-2100F, the heat contents of the CDW layer on the Amundsen Sea shelf increase by 45 and 109 GJ, respectively, compared to the Present experiment. The enhanced ocean heat delivery by CDW over the Amundsen Sea resulted in higher basal melt rates of the ice shelves, which increase by 25 and 44 Gt yr^{-1} for the total Amundsen Sea ice shelves in EASS-2050F and EASS-2100F relative to the Present simulation, respectively.

Despite increases in the Amundsen Sea ice shelf melting rates in EASS-2050F and EASS-2100F, a reduction in meltwater reaching the Ross Sea shelf is found (Figs. 8g,h). Similar to the WAS experiments, through Ekman transports, weakened easterly winds drive reduced sea level near the coast, reducing the onshore SSH gradient and finally inducing anomalous eastward barotropic flows (Figs. 8a,b). Compared with the WAS simulations, changes in SSH and barotropic currents are more significant in EASS due to greater changes in winds. This further reduces the barotropic westward transport of meltwater from the eastern Amundsen Sea. The amount of meltwater dyes on the Ross Sea shelf decreases by 7.6% and 12.7% in EASS-

https://doi.org/10.5194/egusphere-2026-13
Preprint. Discussion started: 14 January 2026

414 2050F and EASS-2100F, respectively. As a result of the reduced freshwater input to the Ross
415 Sea and increased salinity in this region, the DSW volume over the Ross Sea shelf increases
416 by 4.6% in EASS-2050F and 5.3% in EASS-2100F (Table 3). Such changes are not as
417 significant as those in the Ross and WAS experiments, possible because of the large distance
418 from the eastern Amundsen Sea to the Ross Sea.

419 **3.4 Total changes in DSW formation caused by ASL-induced process changes over the**
420 **three regions**

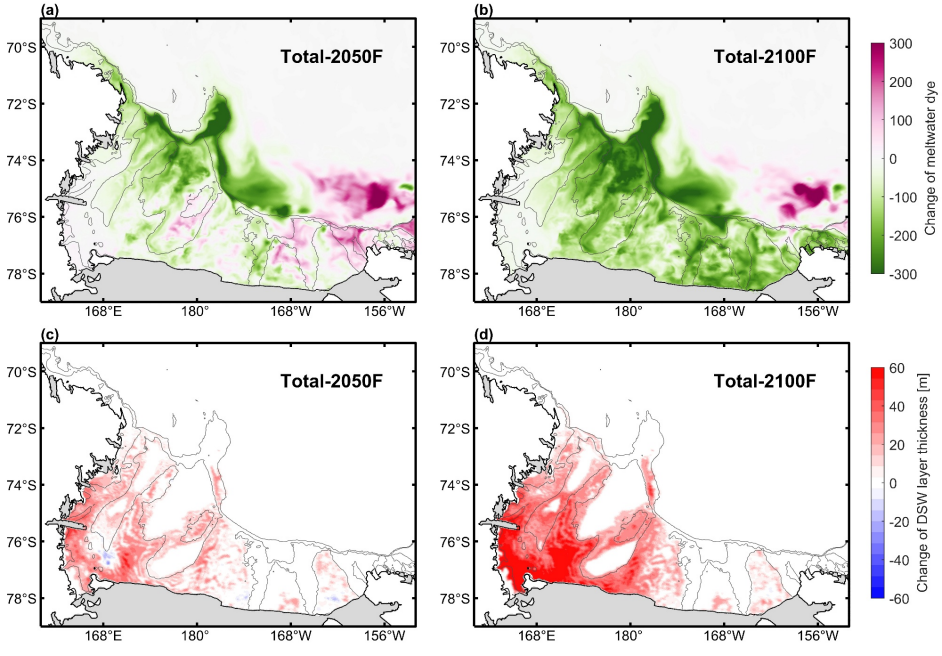

421

422 **Figure 9.** Changes in meltwater dye units in the Ross Sea for the (a) Total-2050F and (b) Total-
423 2100F simulations relative to the Present simulation. Changes in the DSW layer thicknesses
424 for (c) Total-2050F and (d) Total-2100F relative to the Present simulation. Isobaths of 500-m
425 and 1000-m are shown by the black thin line.

https://doi.org/10.5194/egusphere-2026-13
Preprint. Discussion started: 14 January 2026

Due to the complex interactions among processes in the Ross Sea and Amundsen Sea regions, additional experiments are conducted (named Total-2050F and Total-2100F, Table 2) in which wind perturbations associated with the future changes of ASL are applied simultaneously over of the three regions. In Total-2050F and Total-2100F, the amounts of meltwater dye entering the Ross Sea shelf decrease by 10.8% and 28.0%, respectively (Figs. 9a,b). Meanwhile, the sea ice production over the Ross Sea shelf in the two simulations increases by 1.4% and 8.4%, respectively. The reduction in meltwater input and the increase in sea ice production together promote the DSW formation in the Ross Sea, as significant thickening of the DSW layer in the western Ross Sea is observed in Total-2050F and Total-2100F (Figs. 9c,d). The DSW volume on the Ross Sea shelf increases by 7.4% in Total-2050F and 16.8% in Total-2100F (Table 3). The transport of DSW toward the slope across the three transects in the troughs increases by 7.6% and 10.2% in Total-2050F and Total-2100F, respectively. Among the three troughs, the outflow flux in the GCT exhibited the most pronounced increase, contributing 56% and 75% to the total increase in DSW outflow fluxes across the three transects in 2050 and 2100, respectively.

4 Discussion

For the western Amundsen Sea, besides the impact on meltwater transport, Silvano et al. (2020) demonstrated that enhanced easterly winds over this area can increase the sea ice import from the Amundsen Sea into the Ross Sea, increasing sea ice concentration on the Ross Sea shelf and reducing sea ice production and ocean salinity. We found that in WAS-2100F, under the weakened easterly winds, the sea ice import from the Amundsen Sea into the Ross Sea decreases by 15.5% relative to the present period. However, sea ice production over the Ross Sea shelf only shows a slight increase of 1.1% relative to the Present simulation. These findings suggest that the impact of sea ice import from the Amundsen Sea on the Ross Sea DSW

https://doi.org/10.5194/egusphere-2026-13
Preprint. Discussion started: 14 January 2026

formation associated with the ASL change is minor, compared to the impact of meltwater transport.

All simulation results presented in this study focus on annual mean or annual cumulative (e.g. sea ice production) parameters, and do not emphasize seasonality. As sea ice production in the polynyas primarily occurs in March–October, we examined the relationship between ASL indices and wind speed over the Ross Sea shelf during this ice freezing season, and also found a significant negative correlation between the ASL-ACP and the meridional wind component (R=-0.72). Using estimates of the ASL-ACP from the CMIP6-MME10 result, we found that ASL-induced changes in wind speed during the ice freezing season are comparable to that of the annual mean and does not significantly affect our results.

In the Total-2100F simulation, the ASL-induced atmospheric changes over the three study regions could result in a combined increase of 16.8% in 2100. Dinniman et al. (2018) used atmosphere forcing fields from the CMIP3 A1B emissions scenario to drive a coupled ocean-sea ice-ice shelf model for the Ross Sea, and found that the DSW volume will decrease by 18.6%. Using the ensemble-mean atmospheric fields from 21 CMIP6 models under the SSP585 scenario to drive the coupled ocean-sea ice-ice shelf model employed in this study, Xie et al. (2025) showed that the DSW volume in the Ross Sea will decrease by 51% in 2100, as a result of increased freshwater input from the Amundsen Sea and decrease in sea ice production in the Ross Sea polynyas. In such context, the increase in DSW production caused by ASL (16.8%) until the end of this century is important for reducing the current decreasing trend of DSW volume, and for maintaining the AABW production in the Southern Ocean Pacific and Indian sectors.

5 Conclusions

https://doi.org/10.5194/egusphere-2026-13
Preprint. Discussion started: 14 January 2026

473 Climate variability over the West Antarctica region is largely driven by the Amundsen Sea
474 Low and associated wind fields. This study focuses on the impacts of future ASL changes on
475 the formation of DSW — the precursor for AABW in the Ross Sea, Antarctica. In this work,
476 ten models are selected from CMIP6 based on their good performance in simulating the ASL
477 indices, and the ensemble mean of their future projections under the SSP585 scenario are used
478 to derive the ASL changes by the middle and end of the 21st century, as well as the associated
479 wind changes. It is found that the deepening and southward shift of the ASL in the future drive
480 significant anomalous southerly winds over the Ross Sea and westerly winds over the western
481 and eastern Amundsen seas. To quantify how ASL-driven, regionally distinct ocean-sea ice-
482 ice-shelf coupling processes influence DSW formation in the Ross Sea, we conduct sensitivity
483 experiments in which wind anomalies associated with future ASL changes are imposed on each
484 of the three regions.

485 Results from the sensitivity experiments are summarized in Fig. 10. The future deepening
486 of ASL will strengthen southerly winds over the Ross Sea shelf, promoting sea ice production
487 and DSW formation in the Ross Sea polynyas. Meanwhile, in the Amundsen Sea, the future
488 southward shift of ASL will result in reduced easterly winds, decreasing the transport of ice
489 shelf meltwater from the Amundsen Sea to the Ross Sea and thereby promoting the DSW
490 formation. Although the ASL-induced weakening of easterly winds can enhance the melting
491 of Amundsen Sea ice shelves and promote the meltwater release, the significant weakening of
492 barotropic transport of meltwater from the Amundsen Sea to the Ross Sea caused by the wind
493 changes finally leads to more DSW formation in the Ross Sea. These findings highlight the
494 crucial contributions of the future ASL changes to the production of DSW, indicating that the
495 ASL variations can play an inhibitory role in the future diminishing trend of DSW in the Ross
496 Sea, which helps to maintain the AABW production and characteristics in the Pacific and
497 Indian sectors as well as the Southern Ocean meridional overturning circulation.

https://doi.org/10.5194/egusphere-2026-13
Preprint. Discussion started: 14 January 2026

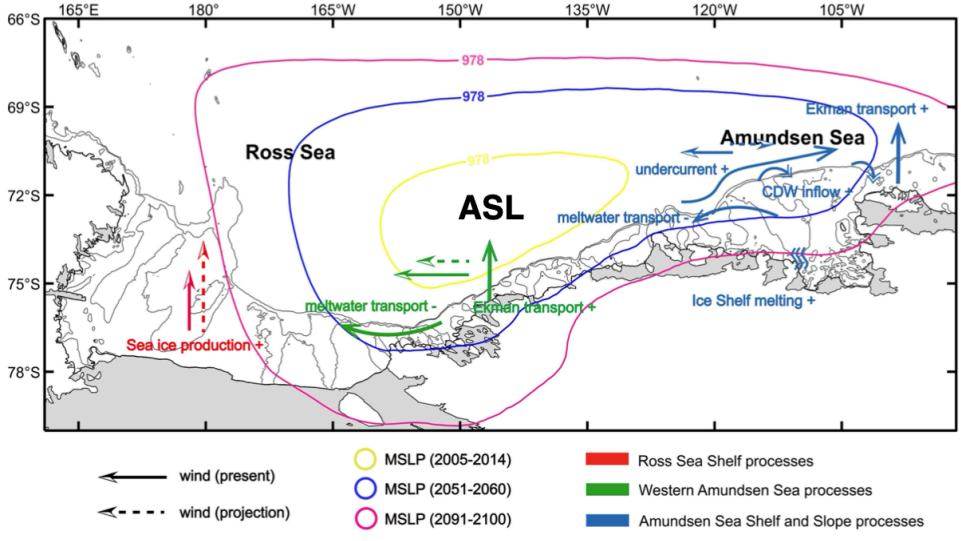

Figure 10. Schematic illustrating the physical mechanisms driving enhanced DSW formation in the Ross Sea caused by future ASL changes. Symbols in red, yellow and blue indicate processes in the Ross Sea, western Amundsen Sea and eastern Amundsen Sea shelf and slope region, respectively. The plus symbol indicates enhancement in the corresponding process, while the minus symbol indicates weakening. Isobaths of 500-m and 1000-m are shown by the black thin lines. In the context of future deepening and poleward migration of the ASL, stronger southerly winds over the Ross Sea will lead to increased sea ice production on the Ross Sea continental shelf. In the western Amundsen Sea, weakened easterly winds will reduce the barotropic transport of ice shelf meltwater from the Amundsen Sea to the Ross Sea. In the eastern Amundsen, weakened easterly winds will enhance CDW intrusion, promoting ice shelf melting, and reducing the westward transport of meltwater. The ultimate effects of these changes are enhancement in the DSW production and export in the Ross Sea.

https://doi.org/10.5194/egusphere-2026-13
Preprint. Discussion started: 14 January 2026

Data availability. The model data that support the findings of this study are available at https://doi.org/10.5281/zenodo.18016271. The ASL indices data are obtained from https://scotthosking.com/asl_index.

Author contributions. ZZ formulated the original ideas presented in this manuscript. ZZ, HH and CX conducted the model results analysis. ZZ and CX wrote the original manuscript draft. HH, XW, YC, CW and CX contributed to the model development, and participated in the result interpretation. All authors contributed to the article and approved the submitted version.

Competing interests. The contact author has declared that none of the authors has any competing interests.

Disclaimer. Publisher's note: Copernicus Publications remains neutral with regard to jurisdictional claims made in the text, published maps, institutional affiliations, or any other geographical representation in this paper. While Copernicus Publications makes every effort to include appropriate place names, the final responsibility lies with the authors.

Acknowledgements. This work is funded by the National Natural Science Foundation of China (Grant No. 42476271), the Shanghai Pilot Program for Basic Research - Shanghai Jiao Tong University (Grant No. 21TQ1400201), and the European Union's Horizon 2020 research and innovation framework programme under Grant agreement no. 101003590 (PolarRES project).

Financial support. This research has been supported by the National Natural Science Foundation of China (grant no. 42476271), the Shanghai Pilot Program for Basic Research of Shanghai Jiao Tong University (grant no. 21TQ1400201), and the European Union's Horizon 2020 research and innovation framework programme under Grant agreement no. 101003590 (PolarRES project).

https://doi.org/10.5194/egusphere-2026-13
Preprint. Discussion started: 14 January 2026

REFERENCES

Bretherton, C. S., Widmann, M., Dymnikov, V. P., Wallace, J. M., and Bladé, I.: The effective number of spatial degrees of freedom of a time-varying field, J. Clim., 12, 1990–2009, https://doi.org/10.1175/1520-0442(1999)012%3C1990:TENOSD%3E2.0.CO;2, 1999.

Bromwich, D. H., and Kurtz, D. D.: Katabatic wind forcing of the Terra Nova Bay polynya, J. Geophys. Res.-Oceans, 89, 3561–3572, https://doi.org/10.1029/JC089iC03p03561, 1984.

Bromwich, D. H., Nicolas, J. P., and Monaghan, A. J.: An Assessment of precipitation changes over Antarctica and the Southern Ocean since 1989 in contemporary global reanalyses, J. Clim., 24, 4189–4209, https://doi.org/10.1175/2011JCLI4074.1, 2011.

Budgell, W. P.: Numerical simulation of ice-ocean variability in the Barents Sea region, Ocean Dyn., 55, 370–387, https://doi.org/10.1007/s10236-005-0008-3, 2005.

Castagno, P., Capozzi, V., DiTullio, G. R., Falco, P., Fusco, G., Rintoul, S. R., Spezie, G., and Budillon, G.: Rebound of shelf water salinity in the Ross Sea, Nat. Commun., 10, 1–6, https://doi.org/10.1038/s41467-019-12049-z, 2019.

Chenoli, S. N., Turner, J., and Samah, A. A.: A strong wind event on the Ross Ice Shelf, Antarctica: A case study of scale interactions, Mon. Weather Rev., 143, 4163–4180, https://doi.org/10.1175/MWR-D-15-0002.1, 2015.

Clem, K. R., Renwick, J. A., and Mcgregor, J.: Large-scale forcing of the Amundsen Sea Low and its influence on sea ice and West Antarctic temperature, J. Clim., 30, 8405–8424, https://doi.org/10.1175/JCLI-D-16-0891.1, 2017.

Coggins, J. H. J., and McDonald, A. J.: The influence of the Amundsen Sea Low on the winds in the Ross Sea and surroundings: Insights from a synoptic climatology, J. Geophys. Res., 120, 2167–2189, https://doi.org/10.1002/2014JD022830, 2015.

https://doi.org/10.5194/egusphere-2026-13
Preprint. Discussion started: 14 January 2026

558 Cohen, L., Dea, S., and Renwick, J.: Synoptic weather types for the Ross Sea region,
559 Antarctica, J. Clim., 26, 636–649, https://doi.org/10.1175/JCLI-D-11-00690.1, 2013.

560 Dale, E. R., McDonald, A. J., Coggins, J. H. J., and Rack, W.: Atmospheric forcing of sea ice
561 anomalies in the Ross Sea polynya region, The Cryosphere, 11, 267–280,
562 https://doi.org/10.5194/tc-11-267-2017, 2017.

563 Depoorter, M. A., Bamber, J. L., Griggs, J. A., Lenaerts, J. T. M., Ligtenberg, S. R. M., Van
564 Den Broeke, M. R., and Moholdt, G.: Calving fluxes and basal melt rates of Antarctic ice
565 shelves, Nature, 502, 89–92, https://doi.org/10.1038/nature12567, 2013.

566 Dinniman, M. S., Klinck, J. M., and Smith, W. O.: A model study of Circumpolar Deep Water
567 on the West Antarctic Peninsula and Ross Sea continental shelves, Deep-Sea Res. Part II,
568 58, 1508–1523, https://doi.org/10.1016/j.dsr2.2010.11.013, 2011.

569 Dinniman, M. S., Klinck, J. M., Bai, L. S., Bromwich, D. H., Hines, K. M., and Holland, D.
570 M.: The effect of atmospheric forcing resolution on delivery of ocean heat to the Antarctic
571 floating ice shelves, J. Clim., 28, 6067–6085, https://doi.org/10.1175/JCLI-D-14-00374.1,
572 2015.

573 Dinniman, M. S., Klinck, J. M., Hofmann, E. E., and Smith, W. O.: Effects of projected changes
574 in wind, atmospheric temperature, and freshwater inflow on the Ross Sea, J. Clim., 31,
575 1619–1635, https://doi.org/10.1175/JCLI-D-17-0351.1, 2018.

576 Dotto, T. S., and coauthors: Variability of the Ross Gyre, Southern Ocean: Drivers and
577 Responses Revealed by Satellite Altimetry, Geophys. Res. Lett., 45, 6195–6204,
578 https://doi.org/10.1029/2018GL078607, 2018.

https://doi.org/10.5194/egusphere-2026-13
Preprint. Discussion started: 14 January 2026

579 Dotto, T. S., and coauthors: Control of the oceanic heat content of the Getz-Dotson Trough,
580 Antarctica, by the Amundsen Sea Low, J. Geophys. Res.-Oceans, 125, e2020JC016113,
581 https://doi.org/10.1029/2020JC016113, 2020.

582 Egbert, G. D., and Erofeeva, S. Y.: Efficient inverse modeling of barotropic ocean tides, J.
583 Atmos. Ocean. Technol., 19, 183–204, https://doi.org/10.1175/1520-
584 0426(2002)019%3C0183:EIMOBO%3E2.0.CO;2, 2002.

585 Fusco, G., Budillon, G., and Spezie, G.: Surface heat fluxes and thermohaline variability in the
586 Ross Sea and in Terra Nova Bay polynya, Cont. Shelf Res., 29, 1887–1895,
587 https://doi.org/10.1016/j.csr.2009.07.006, 2009.

588 Gao, M., Kim, S. J., Yang, J., Liu, J., Jiang, T., Su, B., Wang, Y., and Huang, J.: Historical
589 fidelity and future change of Amundsen Sea Low under 1.5 °C–4 °C global warming in
590 CMIP6, Atmos. Res., 255, 105533, https://doi.org/10.1016/j.atmosres.2021.105533, 2021.

591 Guo, G., Gao, L., and Shi, J.: Modulation of dense shelf water salinity variability in the western
592 Ross Sea associated with the Amundsen Sea Low, Environ. Res. Lett., 16, 014004,
593 https://doi.org/10.1088/1748-9326/abc995, 2021.

594 Haidvogel, D. B., and coauthors: Ocean forecasting in terrain-following coordinates:
595 Formulation and skill assessment of the Regional Ocean Modeling System, J. Comput.
596 Phys., 227, 3595–3624, https://doi.org/10.1016/j.jcp.2007.06.016, 2008.

597 Häkkinen, S., and Mellor, G. L.: Modeling the seasonal variability of a coupled Arctic ice-
598 ocean system, J. Geophys. Res.-Oceans, 97, 20285–20304,
599 https://doi.org/10.1029/92JC02037, 1992.

https://doi.org/10.5194/egusphere-2026-13
Preprint. Discussion started: 14 January 2026

600 Henley, B. J., Gergis, J., Karoly, D. J., Power, S., Kennedy, J., and Folland, C. K.: A Tripole
601 Index for the Interdecadal Pacific Oscillation, Clim. Dyn., 45, 3077–3090,
602 https://doi.org/10.1007/s00382-015-2525-1, 2015.

603 Hersbach, H., and coauthors: The ERA5 global reanalysis, Q. J. R. Meteorol. Soc., 146, 1999–
604 2049, https://doi.org/10.1002/qj.3803, 2020.

605 Holland, D. M., and Jenkins, A.: Modeling thermodynamic ice-ocean interactions at the base
606 of an ice shelf, J. Phys. Oceanogr., 29, 1787–1800, https://doi.org/10.1175/1520-
607 0485(1999)029%3C1787:MTIOIA%3E2.0.CO;2, 1999.

608 Holland, M. M., Landrum, L., Raphael, M. N., and Kwok, R.: The Regional, Seasonal, and
609 Lagged Influence of the Amundsen Sea Low on Antarctic Sea Ice, Geophys. Res. Lett., 45,
610 11227–11234, https://doi.org/10.1029/2018GL080140, 2018.

611 Hosking, J. S., Orr, A., Marshall, G. J., Turner, J., and Phillips, T.: The influence of the
612 Amundsen-Bellingshausen Seas Low on the climate of West Antarctica and its
613 representation in coupled climate model simulations, J. Clim., 26, 6633–6648,
614 https://doi.org/10.1175/JCLI-D-12-00813.1, 2013.

615 Hosking, J. S., Orr, A., Bracegirdle, T. J., and Turner, J.: Future circulation changes off West
616 Antarctica: Sensitivity of the Amundsen Sea Low to projected anthropogenic forcing,
617 Geophys. Res. Lett., 43, 367–376, https://doi.org/10.1002/2015GL067143, 2016.

618 Hunke, E. C.: Viscous-Plastic Sea Ice Dynamics with the EVP Model: Linearization Issues, J.
619 Comput. Phys., 170, 18–38, https://doi.org/10.1006/jcph.2001.6710, 2001.

620 Hunke, E. C., and Dukowicz, J. K.: An elastic-viscous-plastic model for sea ice dynamics, J.
621 Phys. Oceanogr., 27, 1849–1867, https://doi.org/10.1175/1520-
622 0485(1997)027%3C1849:AEVPMF%3E2.0.CO;2, 1997.

https://doi.org/10.5194/egusphere-2026-13
Preprint. Discussion started: 14 January 2026

623 Jacobs, S., Giulivi, C., Dutrieux, P., Rignot, E., Nitsche, F., and Mouginot, J.: Getz Ice Shelf
624 melting response to changes in ocean forcing, J. Geophys. Res.-Oceans, 118, 4152–4168,
625 https://doi.org/10.1002/jgrc.20298, 2013.

626 Jacobs, S. S., and Giulivi, C. F.: Large multidecadal salinity trends near the Pacific-Antarctic
627 continental margin, J. Clim., 23, 4508–4524, https://doi.org/10.1175/2010JCLI3284.1,
628 2010.

629 Jacobs, S. S., Giulivi, C. F., and Mele, P. A.: Freshening of the Ross Sea during the late 20th
630 century, Science, 297, 386–389, https://doi.org/10.1126/science.1069574, 2002.

631 Jacobs, S. S., Jenkins, A., Giulivi, C. F., and Dutrieux, P.: Stronger ocean circulation and
632 increased melting under Pine Island Glacier ice shelf, Nat. Geosci., 4, 519–523,
633 https://doi.org/10.1038/ngeo1188, 2011.

634 Jacobs, S. S., Giulivi, C. F., and Dutrieux, P.: Persistent Ross Sea Freshening From Imbalance
635 West Antarctic Ice Shelf Melting, J. Geophys. Res.-Oceans, 127, e2021JC017808,
636 https://doi.org/10.1029/2021JC017808, 2022.

637 Jendersie, S., Williams, M. J. M., Langhorne, P. J., and Robertson, R.: The Density-Driven
638 Winter Intensification of the Ross Sea Circulation, J. Geophys. Res.-Oceans, 123, 7702–
639 7724, https://doi.org/10.1029/2018JC013965, 2018.

640 Jenkins, A., Shoosmith, D., Dutrieux, P., Jacobs, S., Kim, T. W., Lee, S. H., Ha, H. K., and
641 Stammerjohn, S.: West Antarctic Ice Sheet retreat in the Amundsen Sea driven by decadal
642 oceanic variability, Nat. Geosci., 11, 733–738, https://doi.org/10.1038/s41561-018-0207-
643 4, 2018.

https://doi.org/10.5194/egusphere-2026-13
Preprint. Discussion started: 14 January 2026

644 Kim, C. S., Kim, T. W., Cho, K. H., Ha, H. K., Lee, S. H., Kim, H. C., and Lee, J. H.: Variability
645 of the Antarctic Coastal Current in the Amundsen Sea, Estuar. Coast. Shelf Sci., 181, 123–
646 133, https://doi.org/10.1016/j.ecss.2016.08.004, 2016.

647 Konrad, H., Shepherd, A., Gilbert, L., Hogg, A. E., McMillan, M., Muir, A., and Slater, T.: Net
648 retreat of Antarctic glacier grounding lines, Nat. Geosci., 11, 258–262,
649 https://doi.org/10.1038/s41561-018-0082-z, 2018.

650 Kusahara, K., Williams, G. D., Tamura, T., Massom, R., and Hasumi, H.: Dense shelf water
651 spreading from Antarctic coastal polynyas to the deep Southern Ocean: A regional
652 circumpolar model study, J. Geophys. Res.-Oceans, 122, 6238–6253,
653 https://doi.org/10.1002/2017JC012911, 2017.

654 Large, W. G., McWilliams, J. C., and Doney, S. C.: Oceanic vertical mixing: A review and a
655 model with a nonlocal boundary layer parameterization, Rev. Geophys., 32, 363–403,
656 https://doi.org/10.1029/94RG01872, 1994.

657 De Lavergne, C., Madec, G., Roquet, F., Holmes, R. M., and McDougall, T. J.: Abyssal ocean
658 overturning shaped by seafloor distribution, Nature, 551, 181–186,
659 https://doi.org/10.1038/nature24472, 2017.

660 Li, Z., Wang, C., and Zhou, M.: A model analysis of circumpolar deep water intrusions on the
661 continental shelf break in Amundsen Sea, Antarctica, J. Geophys. Res.-Oceans, 130,
662 e2024JC022210, https://doi.org/10.1029/2024JC022210, 2025.

663 Li, X., Cai, W., Meehl, G., Chen, D., Yuan, X., Raphael, M., Holland, D., Ding, Q., Fogt, R.,
664 Markle, B., Wang, G., Bromwich, D., Turner, J., Xie, S.-P., Steig, E., Gille, S., Xiao, C.,
665 Wu, B., Lazzara, M., and Song, C.: Tropical teleconnection impacts on Antarctic climate
666 changes, Nat. Rev. Earth Environ., 2, 680–698, https://doi.org/10.1038/s43017-021-00204-
667 5, 2021.

https://doi.org/10.5194/egusphere-2026-13
Preprint. Discussion started: 14 January 2026

668 MacLachlan, C., Arribas, A., Peterson, K. A., Maidens, A., Fereday, D., Scaife, A. A., Gordon,
669 M., Vellinga, M., Williams, A., Comer, R. E., Camp, J., Xavier, P., and Madec, G.: Global
670 Seasonal Forecast System version 5 (GloSea5): A high-resolution seasonal forecast system,
671 Q. J. R. Meteorol. Soc., 141, 1072–1084, https://doi.org/10.1002/qj.2396, 2015.

672 Marshall, J., and Speer, K.: Closure of the meridional overturning circulation through Southern
673 Ocean upwelling, Nat. Geosci., 5, 171–180, https://doi.org/10.1038/ngeo1391, 2012.

674 Mellor, G. L., and Kantha, L.: An ice-ocean coupled model, J. Geophys. Res., 94, 10937–
675 10954, https://doi.org/10.1029/JC094iC08p10937, 1989.

676 Morlighem, M., Rignot, E., Mouginot, J., Seroussi, H., Bamber, J. N., Aschwanden, A. A.,
677 Bartholomaus, T. A., Bindschadler, R., Bjørk, G., Brunt, K. M., Chinn, D. N., Paden, J. D.,
678 Fricker, H. A., Jezek, K., Joughin, I., Khan, A., Krabill, W. B., Larsen, A. P., Li, J., Klinger,
679 C. M., Marder, S. R., Millan, B. M., Porter, D. J., Routhier, M. J., Schlegel, M., Smith, B.,
680 Wang, J. Y., Willis, J. J., Williams, G. D., and Winter, J. G.: Deep glacial troughs and
681 stabilizing ridges unveiled beneath the margins of the Antarctic ice sheet, Nat. Geosci., 13,
682 132–137, https://doi.org/10.1038/s41561-019-0510-8, 2020.

683 Nakata, K., Ohshima, K. I., and Nihashi, S.: Mapping of Active Frazil for Antarctic Coastal
684 Polynyas, With an Estimation of Sea-Ice Production, Geophys. Res. Lett., 48,
685 e2020GL091353, https://doi.org/10.1029/2020GL091353, 2021.

686 Nakayama, Y., Schröder, M., and Hellmer, H. H.: From circumpolar deep water to the glacial
687 meltwater plume on the eastern Amundsen Shelf, Deep-Sea Res. Part I, 77, 50–62,
688 https://doi.org/10.1016/j.dsr.2013.04.001, 2013.

689 Nakayama, Y., Timmermann, R., Rodehacke, C. B., Schröder, M., and Hellmer, H. H.:
690 Modeling the spreading of glacial meltwater from the Amundsen and Bellingshausen Seas,
691 Geophys. Res. Lett., 41, 7942–7949, https://doi.org/10.1002/2014GL061600, 2014.

https://doi.org/10.5194/egusphere-2026-13
Preprint. Discussion started: 14 January 2026

692 Naughten, K. A., Meissner, K. J., Galton-Fenzi, B. K., England, M. H., Timmermann, R.,
693 Hellmer, H. H., Hattermann, T., and Debernard, J. B.: Intercomparison of Antarctic ice-
694 shelf, ocean, and sea-ice interactions simulated by MetROMS-iceshelf and FESOM 1.4,
695 Geosci. Model Dev., 11, 1257–1292, https://doi.org/10.5194/gmd-11-1257-2018, 2018.

696 Nicolas, J. P., and Bromwich, D. H.: Climate of West Antarctica and influence of marine air
697 intrusions, J. Clim., 24, 49–67, https://doi.org/10.1175/2010JCLI3522.1, 2011.

698 Nihashi, S., and Ohshima, K. I.: Circumpolar mapping of Antarctic coastal polynyas and
699 landfast sea ice: Relationship and variability, J. Clim., 28, 3650–3670,
700 https://doi.org/10.1175/JCLI-D-14-00369.1, 2015.

701 Núñez-Riboni, I., and Fahrbach, E.: Seasonal variability of the Antarctic Coastal Current and
702 its driving mechanisms in the Weddell Sea, Deep-Sea Res. Part I, 56, 1927–1941,
703 https://doi.org/10.1016/j.dsr.2009.06.005, 2009.

704 Orsi, A. H., and Wiederwohl, C. L.: A recount of Ross Sea waters, Deep-Sea Res. Part II, 56,
705 778–795, https://doi.org/10.1016/j.dsr2.2008.10.033, 2009.

706 Paolo, F. S., Fricker, H. A., and Padman, L.: Volume loss from Antarctic ice shelves is
707 accelerating, Science, 348, 327–331, https://doi.org/10.1126/science.aaa0940, 2015.

708 Park, J., Kim, H. C., Jo, Y. H., Kidwell, A., and Hwang, J.: Multi-temporal variation of the
709 Ross Sea Polynya in response to climate forcings, Polar Res., 37, 1444891,
710 https://doi.org/10.1080/17518369.2018.1444891, 2018.

711 Raphael, M. N., and coauthors: The Amundsen sea low: Variability, change, and impact on
712 Antarctic climate, Bull. Am. Meteorol. Soc., 97, 111–121, https://doi.org/10.1175/BAMS-
713 D-14-00018.1, 2016.

https://doi.org/10.5194/egusphere-2026-13
Preprint. Discussion started: 14 January 2026

714 Raphael, M. N., Holland, M. M., Landrum, L., and Hobbs, W. R.: Links between the Amundsen
715 Sea Low and sea ice in the Ross Sea: seasonal and interannual relationships, Clim. Dyn.,
716 52, 2333–2349, https://doi.org/10.1007/s00382-018-4258-4, 2019.

717 Rignot, E., Jacobs, S., Mouginot, J., and Scheuchl, B.: Ice-shelf melting around Antarctica,
718 Science, 341, 266–270, https://doi.org/10.1126/science.1235798, 2013.

719 Rignot, E., Mouginot, J., Scheuchl, B., Van Den Broeke, M., Van Wessem, M. J., and
720 Morlighem, M.: Four decades of Antarctic ice sheet mass balance from 1979–2017, Proc.
721 Natl. Acad. Sci. U. S. A., 116, 1095–1103, https://doi.org/10.1073/pnas.1812883116, 2019.

722 Rintoul, S. R.: Rapid freshening of Antarctic Bottom Water formed in the Indian and Pacific
723 oceans, Geophys. Res. Lett., 34, L06606, https://doi.org/10.1029/2006GL028550, 2007.

724 Shchepetkin, A. F., and McWilliams, J. C.: Correction and commentary for "Ocean forecasting
725 in terrain-following coordinates: Formulation and skill assessment of the Regional Ocean
726 Modeling System" by Haidvogel et al., J. Comput. Phys., 228, 8985–9000,
727 https://doi.org/10.1016/j.jcp.2009.09.002, 2009.

728 Shepherd, A., Ivins, E., Rignot, E., Smith, B., van den Broeke, M., and Velicogna, I.: Mass
729 balance of the Antarctic Ice Sheet from 1992 to 2017, Nature, 558, 219–222,
730 https://doi.org/10.1038/s41586-018-0179-y, 2018.

731 Sigman, D. M., and Boyle, E. A.: Glacial/interglacial variations in atmospheric carbon dioxide,
732 Nature, 407, 859–869, https://doi.org/10.1038/35038000, 2000.

733 Silvano, A., Rintoul, S. R., Peña-Molino, B., Hobbs, W. R., van Wijk, E., Aoki, S., Tamura,
734 T., and Williams, G. D.: Freshening by glacial meltwater enhances melting of ice shelves
735 and reduces formation of Antarctic Bottom Water, Sci. Adv., 4, eaap9467,
736 https://doi.org/10.1126/sciadv.aap9467, 2018.

https://doi.org/10.5194/egusphere-2026-13
Preprint. Discussion started: 14 January 2026

737 Silvano, A., and coauthors: Recent recovery of Antarctic Bottom Water formation in the Ross
738 Sea driven by climate anomalies, Nat. Geosci., 13, 780–786,
739 https://doi.org/10.1038/s41561-020-00655-3, 2020.

740 Silvano, A., and coauthors: Baroclinic Ocean Response to Climate Forcing Regulates Decadal
741 Variability of Ice-Shelf Melting in the Amundsen Sea, Geophys. Res. Lett., 49,
742 e2022GL100646, https://doi.org/10.1029/2022GL100646, 2022.

743 Spreen, G., Kaleschke, L., and Heygster, G.: Sea ice remote sensing using AMSR-E 89-GHz
744 channels, J. Geophys. Res., 113, C02S03, https://doi.org/10.1029/2005JC003384, 2008.

745 Tamura, T., Ohshima, K. I., Fraser, A. D., and Williams, G. D.: Sea ice production variability
746 in Antarctic coastal polynyas, J. Geophys. Res.-Oceans, 121, 2967–2979,
747 https://doi.org/10.1002/2015JC011537, 2016.

748 Tewari, K., Mishra, S. K., Salunke, P., and Dewan, A.: Future projections of temperature and
749 precipitation for Antarctica, Environ. Res. Lett., 17, 014029, https://doi.org/10.1088/1748-
750 9326/ac43e2, 2022.

751 Thoma, M., Jenkins, A., Holland, D., and Jacobs, S.: Modelling Circumpolar Deep Water
752 intrusions on the Amundsen Sea continental shelf, Antarctica, Geophys. Res. Lett., 35, 2–
753 7, https://doi.org/10.1029/2008GL034939, 2008.

754 Treasure, A. M., and coauthors: Marine Mammals Exploring the Oceans Pole to Pole: A
755 Review of the MEOP Consortium, Oceanography, 30, 132–138,
756 https://doi.org/10.5670/oceanog.2017.234, 2017.

757 Turner, J., Phillips, T., Hosking, J. S., Marshall, G. J., and Orr, A.: The Amundsen Sea Low,
758 Int. J. Climatol., 33, 1818–1829, https://doi.org/10.1002/joc.3558, 2013.

https://doi.org/10.5194/egusphere-2026-13
Preprint. Discussion started: 14 January 2026

759 Xie, C., Zhang, Z., Chen, Y., and Wang, C.: Substantial contraction of dense shelf water in the
760 Ross Sea under future climate scenarios, Geophys. Res. Lett., 52, e2024GL112581,
761 https://doi.org/10.1029/2024GL112581, 2025.

762 Xie, C., Zhang, Z., Chen, Y., Wang, C., and Zhou, M.: The response of Ross Sea shelf water
763 properties to enhanced Amundsen Sea ice shelf melting, J. Geophys. Res.-Oceans, 129,
764 e2024JC020919, https://doi.org/10.1029/2024JC020919, 2024.

765 Wåhlin, A. K., and coauthors: Variability of warm deep water inflow in a submarine trough on
766 the Amundsen Sea shelf, J. Phys. Oceanogr., 43, 2054 – 2070, https://doi.org/10.1175/JPO-
767 D-12-0157.1, 2013.

768 Wang, S., Liu, J., Cheng, X., Yang, D., Kerzenmacher, T., Li, X., Hu, Y., and Braesicke, P.:
769 Contribution of the deepened Amundsen sea low to the record low Antarctic sea ice extent
770 in February 2022, Environ. Res. Lett., 18, 054002, https://doi.org/10.1088/1748-
771 9326/acc9d6, 2023.

772 Wang, T., Wei, H., and Xiao, J.: Dynamic linkage between the interannual variability of the
773 spring Ross Ice Shelf Polynya and the atmospheric circulation anomalies, Clim. Dyn., 53,
774 831 – 840, https://doi.org/10.1007/s00382-021-05936-0, 2022.

775 Wang, X., Zhang, Z., Wang, X., Vihma, T., Zhou, M., Yu, L., Uotila, P., and Sein, D. V.:
776 Impacts of strong wind events on sea ice and water mass properties in Antarctic coastal
777 polynyas, Clim. Dyn., 57, 3505 – 3528, https://doi.org/10.1007/s00382- 021-05878-7,
778 2021.

779 Wang, X., Zhang, Z., Dinniman, M. S., Uotila, P., Li, X., and Zhou, M.: The response of sea
780 ice and high-salinity shelf water in the Ross Ice Shelf Polynya to cyclonic atmosphere

https://doi.org/10.5194/egusphere-2026-13
Preprint. Discussion started: 14 January 2026

781 circulations, The Cryosphere, 17, 1107–1126, https://doi.org/10.5194/tc-17-1107-2023,
782 2023.

783 Weber, N. J., Lazzara, M. A., Keller, L. M., and Cassano, J. J.: The extreme wind events in the
784 Ross Island region of Antarctica, Weather Forecast., 31, 985 – 1000,
785 https://doi.org/10.1175/WAF- D-15-0125.1, 2016.

786 van Wijk, E. M., and Rintoul, S. R.: Freshening drives contraction of Antarctic Bottom Water
787 in the Australian Antarctic Basin, Geophys. Res. Lett., 41, 1657–1664,
788 https://doi.org/10.1002/2013GL058921, 2014.

789 Zhang, X., Hetland, R. D., Marta-Almeida, M., and Dimarco, S. F.: A numerical investigation
790 of the Mississippi and Atchafalaya freshwater transport, filling and flushing times on the
791 Texas-Louisiana Shelf, J. Geophys. Res.-Oceans, 117, 1–21,
792 https://doi.org/10.1029/2012JC00810, 2012.

793 Zhang, Z., Xie, C., Castagno, P., England, M. H., Wang, X., Dinniman, M. S., Silvano, A.,
794 Wang, C., Zhou, L., Li, X., Zhou, M., and Budillon, G.: Evidence for large-scale climate
795 forcing of dense shelf water variability in the Ross Sea, Nat. Commun., 15, 8190,
796 https://doi.org/10.1038/s41467-024-52524-x, 2024.

797 Zhang, Z., Xie, C., Wang, C., Chen, Y., Hu, H., and Wang, X.: The Ross Sea and Amundsen
798 Sea Ice–Sea Model (RAISE v1.0): A high-resolution ocean–sea ice–ice shelf coupling
799 model for simulating the dense shelf water and Antarctic Bottom Water in the Ross Sea,
800 Antarctica, Geosci. Model Dev., 18, 1375–1393, https://doi.org/10.5194/gmd-18-1375-
801 2025, 2025.

https://doi.org/10.5194/egusphere-2026-13
Preprint. Discussion started: 14 January 2026

802 Zhang, Z., Vihma, T., Stössel, A., and Uotila, P.: The role of wind forcing from operational
803 analyses for the model representation of Antarctic coastal sea ice, Ocean Model., 94, 95 –
804 111 http://dx.doi.org/10.1016/j.ocemod.2015.07.019, 2015.

805

806